2013

Numerical Analysis of the Dynamics in Gas-Solid Fluidized Beds and Experimental Validation Using Ultra-Fast X-ray Tomography

Vikrant Verma
Eindhoven University of Technology, Netherlands

Niels G. Deen
Eindhoven University of Technology, Netherlands

Johan T. Padding
Eindhoven University of Technology, Netherlands

J.A.M. Kuipers
Eindhoven University of Technology, Netherlands

Martina Bieberle
Institute of Fluid dynamics, Helmholtz-Zentrum Dresden-Rossendorf e. V., Germany

See next page for additional authors

Authors
Vikrant Verma, Niels G. Deen, Johan T. Padding, J.A.M. Kuipers, Martina Bieberle, Frank Barthel, Michael Wagner, and Uwe Hampel

NUMERICAL ANALYSIS OF THE DYNAMICS IN GAS-SOLID FLUIDIZED BEDS AND EXPERIMENTAL VALIDATION USING ULTRA-FAST X-RAY TOMOGRAPHY

Vikrant Verma[a], Niels G. Deen[a*], Johan T.Padding[a], J.A.M. Kuipers[a],
Martina Bieberle[b], Frank Barthel[b], Michael Wagner[b], and Uwe Hampel[b]
[a]Eindhoven University of Technology; Dept. Chemical Engineering and Chemistry
PO Box 513, 5600 MB Eindhoven, The Netherlands.
[b]Institute of Fluid dynamics, Helmholtz-Zentrum Dresden-Rossendorf e. V.,
PO Box 510119, 01314 Dresden, Germany
*T: 31-40-247-3681; F: 31-40-247-5833; E: N.G.Deen@tue.nl

ABSTRACT

Bubble characteristics in a cylindrical gas-solid fluidized bed have been studied with a two-fluid model (TFM) based on the Kinetic Theory of Granular Flow and validated with experiments performed with X-ray computed tomography (XRT). It is shown that the equivalent bubble diameter increases with height from the gas distributor plate. Experimental and TFM results are in good agreement for glass particles. Darton et al. (1) and Werther (2) correlation slightly over-predict the bubble size. XRT and simulations results show similar trends for LLDP and glass particles. The KTGF theory performs better for glass particles, and is in good agreement with XRT results.

INTRODUCTION

Gas-solid fluidized beds are extensively used in process industries because of their excellent mixing, heat and mass transfer capabilities. They are currently used in separation, classification, drying and mixing of particles, chemical reactions, and regeneration processes. Understanding of the formation and propagation of gas bubbles is the key to scale-up gas-solid fluidized bed reactors. Bubbles grow while moving through the bed mainly because of coalescence. This phenomenon is affected by the particle properties and operating conditions. Many studies (1,2, among others) have been reported in literature, providing correlations for bubble size in the fluidized beds. One of the most popular bubble size correlations was developed by Darton et al. (1), who suggested a correlation based on the bubble growth due to coalescence of bubbles. They assumed that the coalescence occurs inside successive stages along the bed. Their model predicts a continuously increasing bubble size, due to neglect of bubble splitting and breakage. Werther (2) studied the effect of bed diameter on bubble size. So far, most of the studies have focused on comparing correlations and experiments involving pseudo 2D or 2D systems. However, very little work has been reported in full three dimensional systems. Study of fully

three dimensional fluidized beds is still a challenge; numerically due to high computational cost and experimentally because flow visualization and measurements are difficult to perform. X-ray tomographic techniques are gaining more attention in the research for flow visualization (3,4,5). It can provide planar solid distribution profiles in a fluidized bed without disturbing the internal flow (3). Hulme and Kantzas (4) and Franka and Heindel (5) studied bubble characteristics and gas holdup respectively using X-ray technique. Recently Bieberle, et al. (6) and Mudde (7) showed the large potential of this technique to study gas-solid flow. To investigate the bubble behavior in three dimensional bed numerically, the two-fluid model (TFM) based on Kinetic Theory of Granular Flow (KTGF) has been developed. In this model both phases are treated as interpenetrating continua, where the KTGF is used to provide closures for representation of particle-particle interactions. Although the TFM has been extensively studied in literature (8), it has mainly been used for 2D simulations, due to computational and numerical complexities. In our work, a highly efficient numerical approach was developed and implemented for the solution of the governing equations on a 3D cylindrical staggered grid. Experimental validation of simulation results were achieved using an ultrafast X-ray computed tomography (XRT) technique. Both experiments and simulations were performed on a bubbling fluidized bed with a diameter of 0.1 m.

This paper is organized as follows. First a short description of the TFM is given focusing on the governing equations. Subsequently, the experimental set up and procedure is explained, followed by a discussion of the results, including a comparison of the experimental and numerical results with literature correlations.

TWO-FLUID MODEL

The TFM describes both the gas phase and the solid phase as fully interpenetrating continua using a generalized form of the Navier-Stokes equations for interacting continua.
Continuity equation (symbols used are explained in notation section):

$$\frac{\partial(\varepsilon_g \rho_g)}{\partial t} + \nabla \cdot \left(\varepsilon_g \rho_g \bar{u}_g \right) = 0 \tag{1}$$

$$\frac{\partial(\varepsilon_s \rho_s)}{\partial t} + \nabla \cdot \left(\varepsilon_s \rho_s \bar{u}_s \right) = 0 \tag{2}$$

Momentum equations:

$$\frac{\partial(\varepsilon_g \rho_g \bar{u}_g)}{\partial t} + \nabla \cdot \left(\varepsilon_g \rho_g \bar{u}_g \bar{u}_g \right) = -\varepsilon_g \nabla p_g - \nabla \cdot \left(\varepsilon_g \bar{\bar{\tau}}_g \right) - \beta \left(\bar{u}_g - \bar{u}_s \right) + \varepsilon_g \rho_g \bar{g} \tag{3}$$

$$\frac{\partial(\varepsilon_s \rho_s \bar{u}_s)}{\partial t} + \nabla \cdot \left(\varepsilon_s \rho_s \bar{u}_s \bar{u}_s \right) = -\varepsilon_s \nabla p_g - \nabla p_s + \nabla \cdot \left(\varepsilon_s \bar{\bar{\tau}}_s \right) + \beta \left(\bar{u}_g - \bar{u}_s \right) + \varepsilon_s \rho_s \bar{g} \tag{4}$$

To describe the particle-particle interactions the KTGF is used, which expresses the isotropic and deviatoric parts of the solids stress tensor (i.e. the solids pressure and solids viscosities) as a function of the granular temperature defined as:

$$\Theta = \frac{1}{3} < \bar{C}_s \bar{C}_s > \quad (5)$$

In this work the constitutive equations by Nieuwland et al. (9) have been used. The granular temperature evolves according to:

$$\frac{3}{2}\left[\frac{\partial}{\partial t}\left(\varepsilon_s \rho_s \Theta\right) + \nabla \cdot \left(\varepsilon_s \rho_s \Theta \bar{u}_s\right)\right] = -\left(p_s \bar{\bar{I}} + \varepsilon_s \bar{\bar{\tau}}_s\right) : \nabla \bar{u}_s - \nabla \cdot \left(\varepsilon_s q_s\right) - 3\beta\Theta - \gamma \quad (6)$$

EXPERIMENTAL SETUP AND PROCEDURE

A schematic representation of the experimental setup is shown in Figure 1. The cylindrical fluidized bed is made of transparent polycarbonate with an inner bed diameter of 0.1 m. The overall column height is 1.4 m. Sequences of the cross-sectional density distribution within the column were acquired using ultra-fast X-ray tomography. Details of XRT setup and measurements can be found in Fischer and Hampel (10). Spherical low linear density polyethylene (LLDP) particles (diameter 0.7-1.3 mm) or glass particles (diameter 1.0 mm) falling in Geldart B classification were filled into the column from the top. Subsequently, measurements were performed for an initial bed height of 0.1 m (Aspect ratio 1) and 0.2 m (Aspect ratio 2). Pressurized air was fed through the bottom of the column. The air was supplied by a two stage side channel blower, with a maximum capacity of 205 m^3/hr, and a power of 4kW. The air flow rate was controlled by a frequency controller. The internal wall of the column was partly covered with very thin aluminum tape, and the fluidization air was humidified to ~60% relative humidity to prevent any electrostatic charging.

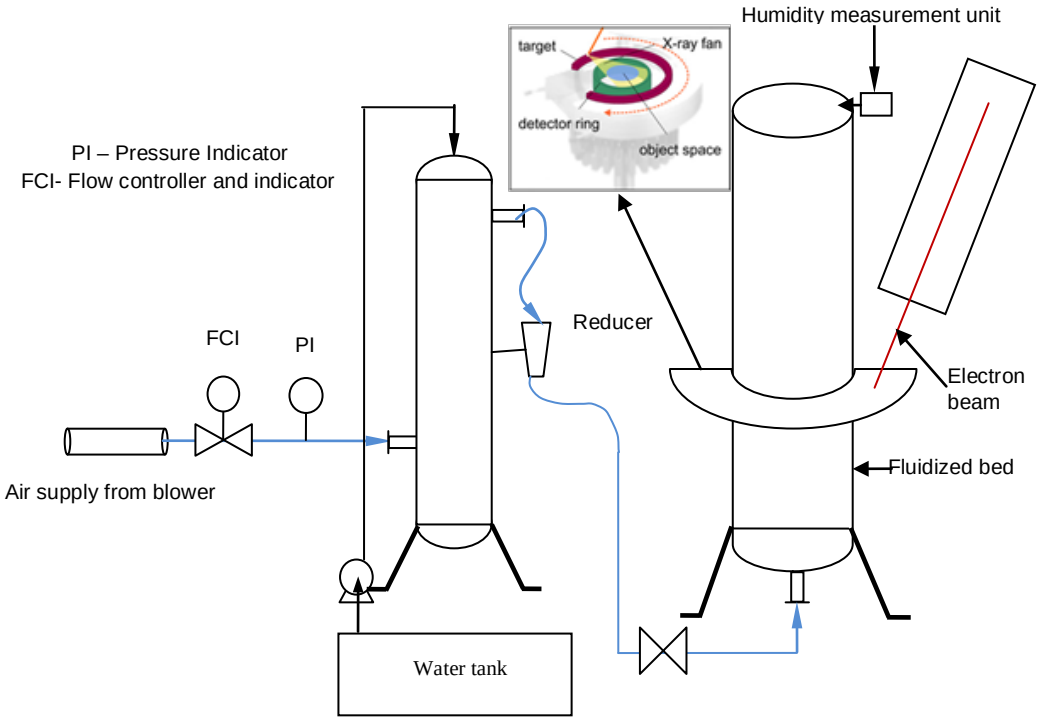

Figure 1: Sketch of X-ray tomography on fluidized beds; experimental setup.

Measurements were performed for a gas flow rate equal to 1.5 times its minimum fluidization velocity, at a spatial resolution of 1 mm, and a temporal resolution of 1000 cross sectional images per second using X-ray tomography (XRT) setup. X-ray CT scanning was performed for 20 s each with 25 mA beam current, at different heights above the gas distributor plate. A detailed discussion on XRT measurements techniques using same setup is presented by Fischer and Hampel (10)

Data Post processing technique: Raw-images of the fluidized bed generated from XRT were reconstructed with help of in-house software using filtered back projection method. The equivalent bubble diameter is calculated from reconstructed images using image processing tool box in MATLAB. A similar algorithm is developed in C program to detect bubbles in our TFM simulation data. The only difference between the two approaches is that for XRT, MATLAB uses a local threshold value using Otsu's method for individual images and a noise removing step is added. In TFM, a gas fraction greater than 0.8 is assumed to be a bubble. For comparison, the TFM simulation data for the initial 1 s have been disregarded due to startup effect.

Table 1: TFM simulation and experimental (XRT) settings

Property	**Value**		**Unit**
	TFM	**XRT**	
Radius	0.05 (20 cells)	0.05	m
Azimuthal angle	2π (20 cells)	2π	radian
Particle Bed height (AR=1)	0.10 (40 cells)	0.10	m
Particle Bed height (AR=2)	0.20 (80 cells)	0.20	m
Time step	10^{-4}	-	s
Total time	20	20	s
Pores in gas distributor plate	-	0.7	mm
Drag force model	Van der Hoef (11)	-	-
Frictional Viscosity model	Srivastava & Sundaresan (8)	-	-

RESULTS AND DISCUSSION

The influence of the particle properties on the equivalent bubble diameter has been investigated. Details on the TFM simulations and XRT experimental settings can be found in Table 1. Properties of particles are presented in Table 2. Figure 2 shows selected reconstructed images of bubbles captured using XRT. Different bubble shapes are detected, ranging from approximately spherical to very irregular shapes. Coalescence and breakup was observed in image sequences as well as in the TFM simulations. Chaotic motion of bubbles was observed in the animations of the TFM simulation results and can also be seen

from the contour plots in Figure 3. Small bubbles emerge near the column wall and move towards the center due to the lower resistance in the center, leading to the formation of larger bubbles. Eruption of larger bubbles into the free board region generally takes place from the center of the bed.

Table 2: Particle properties

Type	Density (kg/m^3)	Diameter (mm)	U_{mf} (m/s)	e_n (TFM)
Glass	2526	1.0 (XRT: 0.7-1.3)	0.68	0.97
LLDP	800	1.0 (XRT: 1.0)	0.26	0.80

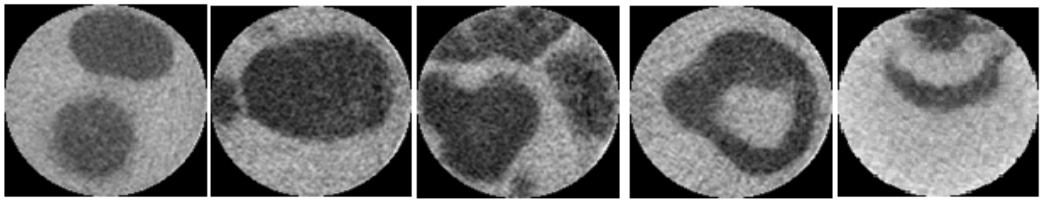

(a) (b) (c) (d) (e)

Figure 2: Different shapes of bubbles observed experimentally in the cross-sectional planes during fluidization. (a) Small spherical bubbles, (b) large spherical bubbles, (c) irregular bubbles, (d) spherical cap bubbles, and (e) arcs (wakes).

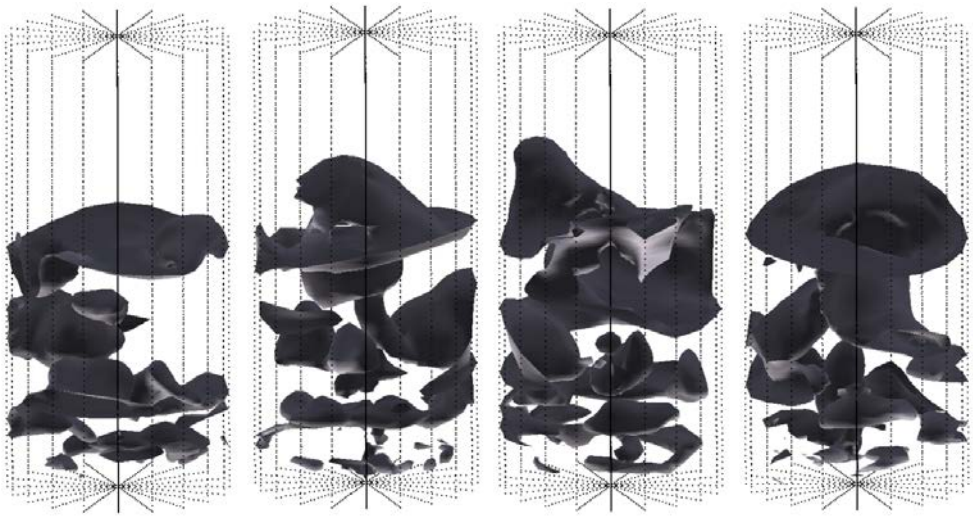

(a) (b) (c) (d)

Figure 3: Simulated 3-D contours plot of bubbles for LLDP particles fluidizing at $1.5U_{mf}$ (a) 2.0 s (b) 4.0 s (c) 6.0 s (d) 8.0 s from the start of fluidization.

Figures 4 and 5 show the development of the equivalent bubble diameter along the height from the gas distributor plate, for LLDP and glass particles. Here equivalent bubble diameter is defined, assuming circular area of each bubble in the cross-sectional plane. The equivalent bubble diameter increases with the

height because of coalescence of smaller bubbles and exchange of gas from emulsion phase. A constant increasing trend in the bubble diameter is observed both experimentally and numerically, which is in fair agreement with literature correlations. Only the Darton correlation with a zero catchment area (A_0 in their correlation; a zero initial bubble size is assumed for a porous plate) predicts a bubble size in agreement with TFM and XRT in the bottom section of the fluidized beds. The correlation of Werther overestimates the bubble size, maybe due to the fact that this correlation was developed for fine particles (sand) and a bed diameter greater than 45 cm. TFM and XRT results are in close agreement in the case of glass particles (Figure 5). Some deviation between XRT measurements and TFM simulations is observed for LLDP particles (Figure 4). Figure 6(a) and (b) reveals that frequencies of bubbles observed in XRT measurements are different for both types of particles. Bubble size distribution for glass particles (figure 6(b)) shows close fit for XRT and TFM simulations. For glass particles, very small and large bubbles are observed both in TFM and XRT.

However for LLDP particles smaller bubble are not observed in the XRT measurements. The reason may be that smaller bubbles are difficult to distinguish with the XRT technique for low density particles. The low contrast associated with low density particles, the image processing algorithm used here fails to detect smaller bubbles. Moreover, much larger bubbles are detected with

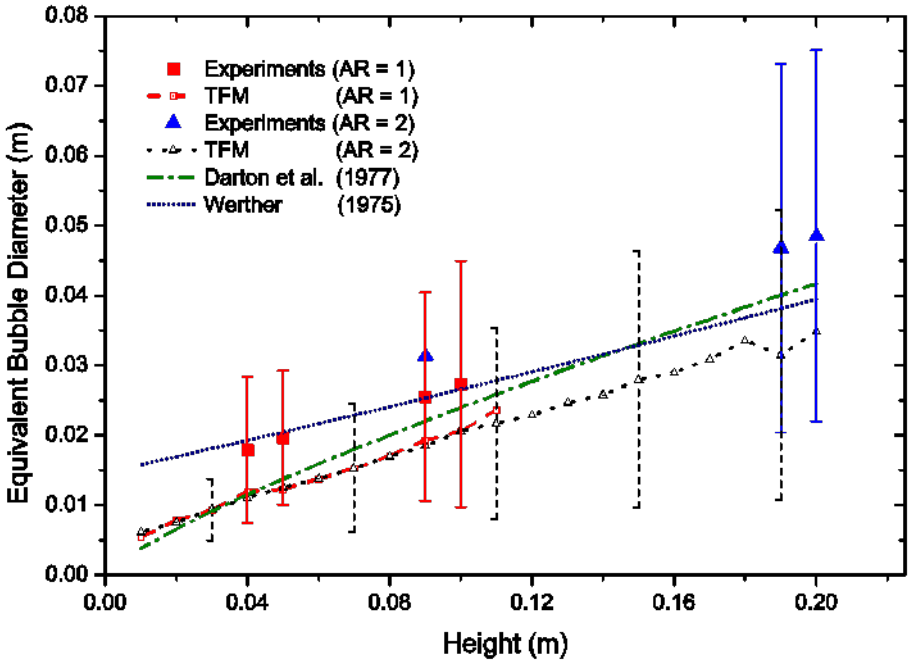

Figure 4: Time-averaged equivalent bubble diameter at different height in the fluidized bed, for fluidization of LLDP particles at $1.5U_{mf.}$ Vertical bars represent standard deviation in the measured (solid vertical bar) and TFM (dash vertical bar) bubble diameter.

XRT that are not observed in the TFM simulations. We suspect this apparent behavior is due to particle-particle collision parameters. Experimental values of the collision parameters, particularly for LLDP particles, are not known very well. In literature (12) coefficients of restitution for LLDP are reported to be much lower than 0.8. In this study, a higher value of 0.80 was used to prevent usage of

unacceptable small time-steps (10^{-6}) that would have to be taken for a stable solution at lower values of the coefficient of restitution. However, we have noticed (not shown here) that lowering this value does not make any significant difference in the bubble size. Goldschmidt et al. (13) studied in detail the effect of the coefficient of restitution in the KTGF based continuum model. They concluded that the continuum model is very sensitive to particle-particle collisions. KTGF is well suited for nearly ideal particles (such as glass beads) and has its limitation for particles with low coefficient of restitution such as LLDP. The error can also be introduced in the experiments, such as air supply, which depends on the properties of the porous plate and fluctuations from air blower. Moreover, for LLDP fluidization, a particle size distribution (0.7-1.3 mm) was used in the experiments, but a constant particle diameter of 1 mm is used in the simulations. This could also cause the disparities in TFM and XRT results for LLDP.

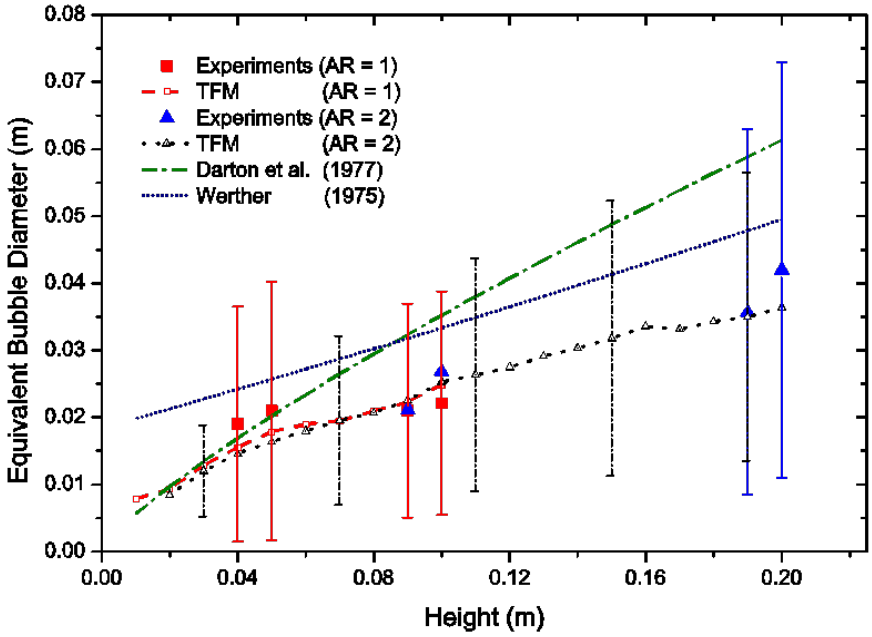

Figure 5: Time-averaged equivalent bubble diameter at different height in the fluidized bed, for fluidization of glass particles at 1.5Umf. Vertical bars represent standard deviation in the measured (solid vertical bar) and TFM (dash vertical bar) bubble diameter.

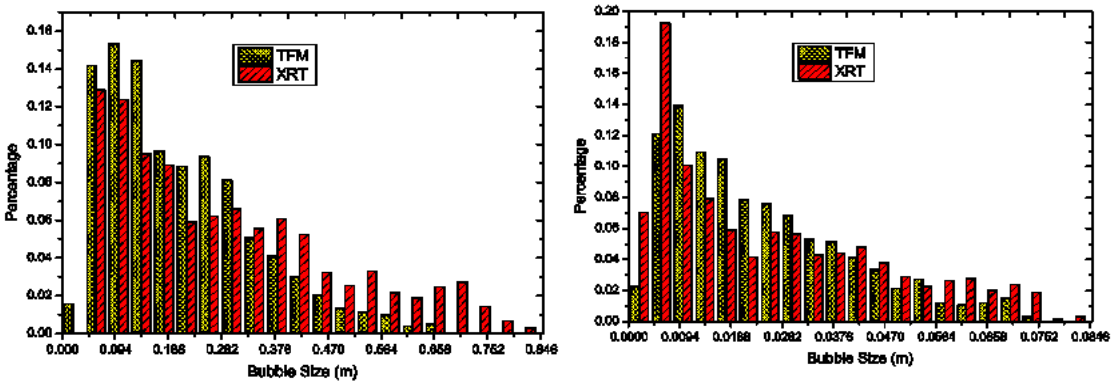

(a) (b)

Figure 6: Distribution of bubbles for different size group at the height of 10 cm from the gas distributor, fluidizing at 1.5Umf. (a) LLDP particles, (b) Glass particles.

The effects of the initial bed height have been investigated both experimentally and numerically. To do this, two different initial bed heights with bed aspect ratio (AR) of 1 and 2 are used. Both systems show almost the same trend in equivalent bubble diameter (see Figure 4 and 5). TFM simulations and XRT measurements show that for these systems the initial particle bed height does not influence the bubble diameter in comparable segments of the bed.

CONCLUSIONS

Bubble diameters as a function of height from distributor plate have been investigated in a 3D gas-solid fluidized bed, both experimentally and numerically for glass and LLDP particles. The equivalent bubble diameter increases with increasing height as bubbles grow and move upward. Chaotic behavior of gas bubbles in the 3D domain is observed, leading to the formation of different bubble shapes and sizes. Smaller bubbles emerge from the bottom grow in size, while moving towards the centerline of the bed. TFM shows better performance for glass particles and a better fit with XRT results. TFM for fluidized bed is dependent upon validity of the KTGF closures. Hence further investigation is required for the KTGF closures, to include particle tangential and rotational friction. Study of the coefficient of restitution and grid refinement may also be of interest for further investigation. Nevertheless this study provides an insight in the behavior of KTGF for different density particles. XRT appears to be a promising technique to study bubble behavior and can act as basic input for coarse grained reactor models of gas-solid fluidized beds.

ACKNOWLEDGMENT

The authors would like to thank the European Research Council for its financial support, under its Advanced Investigator Grant scheme, contract number 247298 (MultiscaleFlows).

NOTATION

C fluctuation particle velocity, $m.s^{-1}$
g gravitational acceleration, $m.s^{-2}$
I unit tensor, -
p pressure, Pa
q kinetic fluctuation energy, $kg.s^{-1}$
u velocity $m.s^{-1}$
t time, s
e_n Coefficient of restitutions, -
U_{mf} Minimum fluidizations velocity, $m.s^{-1}$

Greek symbols

β interphase momentum transfer coefficient, $kg.m^{-3}.s^{-1}$
γ dissipation due to inelastic particles collisions, $kg.m^{-1}.s^{-3}$
ε volume fraction, -
ρ density, kg/s
Θ pseudo particles temperature, $m^2.s^{-2}$
τ stress tensor, Pa

Subscripts

s solid phase
g gas phase

REFERENCES

1. R.C. Darton, R.D. La Naueza, J.F. Davidson, D. Harrison, Bubble growth due to coalescence in fluidized beds, Trans. Inst. Chem. Eng. 55 (1977) 274–280.
2. J. Werther, Bubble growth in a large diameter fluidized beds, Int. Fluidization conference, Pacific Grove, USA, 1975, in: D.L, Keairns (Ed.), Fluidization Technology, Hemisphere Publ. Co., Washington DC, 1976, pp. 215-235.
3. Grassler, T. and K. E. Wirth. X-ray computer tomography - potential and limitation for the measurement of local solids distribution in circulating fluidized beds. Chemical Engineering Journal 77(1): 65-72, 2000.
4. Ian Hulme, Apostolos Kantzas. Determination of bubble diameter and axial velocity for a polyethylene fluidized bed using X-ray fluoroscopy. Powder Technology 147: 20-33, 2004.
5. Nathan P. Franka, Theodore J. Heindel. Local time-averaged gas holdup in a fluidized bed with side air injection using X-ray computed tomography. Powder Technology 193: 69-78, 2009.
6. M. Bieberle, et al., Ultrafast X-ray computed tomography for the analysis of gas–solid fluidized beds, Chem. Eng. J. (2012), doi:10.1016/j.cej.2012.02.028
7. R.F. Mudde, Double X-ray tomography of a bubbling fluidized bed, Ind. Eng. Chem. Res. 49 (2010) 5061–5065.
8. A. Srivastava and S. Sundaresan. Analysis of a frictional-kinetic model for gas-particle flow. Powder Technology, 129:72-85, 2003.
9. J.J. Nieuwland, M. Van Sint Annaland, J.A.M. Kuipers, and W.P.M. van Swaaij. Hydrodynamic modeling of gas/particle flow in riser reactors. AIChE Journal, 42:1569-1582, 1996.
10. Fischer and Hampel, Ultra fast electron beam X-ray computed tomography for two-phase flow measurements. Nuclear Engineering and Design 240, 2254–2259, 2010.
11. Van der Hoef, M.A., van Sint Annaland, M. and Kuipers, J.A.M. Computational fluid dynamics for dense gas-solid fluidized beds: a multi-scale modeling strategy, Chem. Eng. Sci., (2004).59, 5157-5165.
12. Blake K. Chandrasekaran, Loni van der Lee, Ian Hulme, Apostolos Kantzas. A simulation and experimental study of the hydrodynamic of bubbling fludized bed of linear low density polyethylene using bubble properties and pressure fluctuations. Macromol. Mater. Eng, 290, 592-608, 2005.
13. M.J.V. Goldschmidt, J.A.M. Kuipers, and W.P.M. van Swaaij. Hydrodynamic modelling of dense gas-fluidised beds using the kinetic theory of granular flow: effect of coefficient of restitution on bed dynamics. Chemical Engineering Science, 56:571-578, 2001.
14. D. Gidaspow. Multiphase flow and fluidization: Continuum and kinetic theory descriptions. Academic Press, Boston, 1994.
15. Laverman, J. A. On the hydrodynamics in gas phase polymerization reactors. Ph.D. Thesis, Eindhoven University of Technology, Eindhoven, The Netherlands, 2010.
16. S. Mori and C.Y. Wen, Estimation of Bubble diameter in gaseous fluidized beds. AIChE Journal, 21:109-115, 1975.